UNIVERSITY
OF TRENTO

DIPARTIMENTO DI INGEGNERIA E SCIENZA DELL'INFORMAZIONE

OPTIMIZED DESIGN OF A MULTI-FUNCTION/MULTI-BAND
ANTENNA FOR AUTOMOTIVE RESCUE SYSTEMS

R. Azaro, F. De Natale, M. Donelli, A. Massa, and E. Zeni

January 2011

Technical Report # DISI-11-085

Optimized Design of a Multi-Function/Multi-Band Antenna for Automotive Rescue Systems

Renzo Azaro, Francesco De Natale, Massimo Donelli, Andrea Massa, and Edoardo Zeni

DEPARTMENT OF INFORMATION AND COMMUNICATION TECHNOLOGY

University of Trento, Via Sommarive 14, 38050 Trento, ITALY

Tel.: +39 0461 882057, Fax: +39 0461 882093

E-mail: {*andrea.massa*, *francesco.denatale*}*@ing.unitn.it*,

   {*renzo.azaro*, *massimo.donelli, edoardo.zeni*}*@dit.unitn.it*,

Web: *http://www.eledia.ing.unitn.it*

Optimized Design of a Multi-Function/Multi-Band Antenna for Automotive Rescue Systems

Renzo Azaro, Francesco De Natale, Massimo Donelli, Andrea Massa, and Edoardo Zeni

Abstract. The development of efficient automotive accident management systems requires the design of complex multi-function antennas enabling different wireless services (e.g., localization, voice and data communications, emergency calls, etc...). Starting from different specifications (electrical, mechanical, and aerodynamic), the design of a multifunction antenna must consider, in addition to the usual antenna design requirements, also interference phenomena arising from the integration of different classes of antennas in a compact device. In this framework, the paper describes a methodology based on a stochastic multi-phases optimization approach for the design of an integrated multi-function/multi-band antenna system. Moreover, for an exhaustive assessment, the results of an experimental validation performed on a prototype of the multi-function antenna system are shown and discussed.

Key Words: Multi-function/Multi-Band Antenna, Antenna Design, Wireless Systems, System Integration, Particle Swarm Optimizer.

1. INTRODUCTION

An efficient accident management system for automotive applications is usually interfaced with several wireless communication systems enabling different functions, such as data exchange with a remote centre, timing, and localization. Nowadays, these functions are offered at low costs by mobile phone networks for voice and data exchange, and by global positioning system (GPS) for timing and localization. Therefore, a system able to fully exploit the available wireless functionalities requires an antenna system operating in different frequency bands. Moreover, because of the specific application in automotive environments, other issues arise concerned with the coexistence of more antennas in a limited area (i.e., the co-site interference phenomena), the limited weight, and the volume constraints.

This paper describes the methodology adopted to design the antenna system within the AIDER (Accident Information and Driver Emergency Rescue) project[1]. The main objective of AIDER was the development of an accident management system able to reduce the consequences of a road accident by allowing effective rescue operations. To accomplish this task, AIDER vehicles are equipped with a sensor suite and a data acquisition system aimed at monitoring the pre- and post-crash status of the vehicle as well as its occupants. The system is able to automatically send an emergency call and a complete set of information (e.g., audio, video, and sensor data) about the accident to a remote control centre. Towards this end, a highly survivable communication system, based on the integration of the functions of a cellular and a backup satellite communication link (GSM/GPRS and COSPAS-SARSAT system), is provided for the information exchange between vehicle and rescue center. In addition, each AIDER vehicle is equipped with a GPS receiver in order to precisely locate the position of the car.

The design of an antenna for each wireless subsystem (COSPAS-SARSAT, GPS, GSM/GPRS) is not critical in itself, there being available a large number of commercial

---

devices on the market. Nevertheless, the design of an integrated antenna requires great care to guarantee all links to multiple wireless services by avoiding mutual coupling effects arising when the radiating subsystems have to be placed in a single limited volume.

Starting from the electrical guidelines of the rescue system and by taking into account the geometrical constraints arising from integration in a single compact volume within the body of the car, the antenna design has been carried out through a three phase strategy described more in detail in the following section (Sect. 2). Such a design procedure is based on the use of a standard full-wave simulator (based on a Method-of-Moment code or on a FDTD code) to predict the electromagnetic behavior of each antenna as well as of the integrated system.

To assess the effectiveness and reliability of the optimized system, some prototypes of the multi-function antenna have been developed and tested. In Sect. 3, the results of the experimental validation are reported.

2. ANTENNA SYSTEM OPTIMIZED DESIGN

Let us consider the design of an integrated multi-function antenna operating in different range of frequencies to exploit various wireless services, namely SARSAT, GSM/GPRS, and GPS with the following requirements:

$$G_a\{\theta,\phi,f\} \geq G_a^{\min}\{\theta,\phi,f\}$$
$$f_a^{\min} \leq f \leq f_a^{\max} \qquad (1)$$
$$VSWR_a\{f\} \leq VSWR_a^{\max}$$

f being the working frequency and $a \in \{SRS, GSM/GPRS, GPS\}$; G and $VSWR$ indicate the gain and the voltage-standing-wave-ratio, respectively. From a geometric point-of-view, the antenna system is required to belong to a fixed volume defined as

$$x^{\min} \leq x_a \leq x^{\max}$$
$$y^{\min} \leq y_a \leq y^{\max} \qquad \forall a \qquad (2)$$
$$z^{\min} \leq z_a \leq z^{\max}$$

where $\{x_a, y_a, z_a\}$ identifies a point on the extent of the a-th antenna sub-system.

To solve such a problem, a three-phase process is considered. The first phase, called "*Single-Antenna Type Selection*", is aimed at defining the more appropriate class of antennas for each wireless service by taking into account physical as well as electric constraints. The second phase (i.e., the "*Single-Antenna Optimization*") deals with the design of each antenna subsystem as a stand alone device on a ground plane. Then, starting from the solutions defined at the second step, the "*Integrated-Antenna Optimization*" refines the integrated system to define the optimal geometric placement of the different antennas sub-systems and to solve interference problems. The last two phases were both carried out through an optimization procedure.

More in detail:

Single-Antenna Type Selection

Within an automotive framework, antenna systems are commonly installed on roof of the vehicle. This can be modeled by considering an infinite ground plane located at $z^{\min} = 0.0$. Moreover, to guarantee reduced weight, dimensions and aerodynamic properties of the integrated antenna and to simplify the integration phase of the different subsystems in a single device, it could be profitable to consider only wire structures. On the other hand, the electric and physical requirements specified in (1) and (2) define some constraints on the most suitable classes of antennas.

As far as the COSPAS-SARSAT and the GSM/GPRS systems are concerned, a monopole antenna turns out to be a good choice. On the other hand, the GSM/GPRS system operates in two different frequency bands. Therefore, a dual-band monopole antenna might be adopted by considering a LC tuning device allowing multi-band operations.

A more demanding task is related to the selection of a proper antenna subsystem for the GPS function, since the possibility to exactly locate a vehicle in an after-crash status is a crucial task for optimizing the rescue management in terms of time and effectiveness.

In order to improve the GPS receiver performance, some key points should be considered. An enhancement of the effectiveness of a GPS receiver can be obtained either by reducing the effects of multi-path phenomena caused by reflections, or

achieving a hemispherical coverage to receive signals from a large number of satellites. A good solution is represented by a right-hand polarized antenna with a good cross polarization rejection ratio able to discriminate between direct and reflected signals. A large number of commercial GPS receivers employ low-cost/light-weight patch antennas, since the arising radiation patterns presents a wide lobe and a circular polarization with a proper feed arrangement. Unfortunately, patch antennas are narrow-band devices and the resonant frequency varies depending on the ground plane size as well as on the dielectric loading [1].

On the other hand, helical and spiral antennas radiate a circular-polarized field on a wide frequency band. Moreover, such structures are relatively insensitive to mutual coupling phenomena [2] [3] and they present a wide hemispherical lobe as well as good cross-polarization-rejection-ratios [4] [5] [6] [7] [8]. Accordingly, a conical version of the so-called two-arm Archimedean spiral antenna is chosen as reference structure.

Single-Antenna Optimization

According to the guidelines defined in the "*Single-Antenna Type Selection*" phase, the original problem is recast in the following one "*defining the physical parameters of each antenna sub-system to fit the electrical requirements in each frequency band*". Analytically, (1) reformulates as follows

$$G_{SRS}\{\theta,\phi,f\} = \Phi_{SRS}(l_{SRS},d_{SRS}) \geq G_{SRS}^{\min}\{\theta,\phi,f\}$$

$$f_{SRS}^{\min} \leq f \leq f_{SRS}^{\max} \quad (3)$$

$$VSWR_{SRS}\{f\} = \Psi_{SRS}(l_{SRS},d_{SRS}) \leq VSWR_{SRS}^{\max}$$

l_{SRS} and d_{SRS} being the length and the wire-diameter of the COSPAS-SARSAT monopole, respectively;

$$G_{GSM}\{\theta,\phi,f\} = \Phi_{GSM}\left(l_{GSM}^{(1)},l_{GSM}^{(2)},d_{GSM},L,C\right) \geq G_{GSM}^{\min}\{\theta,\phi,f\}$$

$$f_{GSM}^{(1)\min} \leq f \leq f_{GSM}^{(1)\max}, \quad f_{GSM}^{(2)\min} \leq f \leq f_{GSM}^{(2)\max}$$

$$VSWR_{GSM}\{f\} = \Psi_{GSM}\left(l_{GSM}^{(1)},l_{GSM}^{(2)},d_{GSM},L,C\right) \leq VSWR_{GSM}^{\max}$$

$$(4)$$

where $l_{GSM}^{(1)}$ and d_{GSM} are the whole length and the diameter of the dual-band monopole, respectively, while $l_{GSM}^{(2)}$ indicates the vertical position along the monopole where the tuning circuit is located; L and C being the values of the lumped components of the tuning circuit;

$$G_{GPS}\{\theta,\phi,f\} = \Phi_{GPS}\left(r_{GPS}^{(1)}, r_{GPS}^{(2)}, h_{GPS}^{(1)}, h_{GPS}^{(2)}, S_{GPS}, d_{GPS}\right) \geq G_{GPS}^{\min}\{\theta,\phi,f\}$$

$$f_{GPS}^{\min} \leq f \leq f_{GPS}^{\max}$$

$$VSWR_{GPS}\{f\} = \Psi_{GPS}\left(r_{GPS}^{(1)}, r_{GPS}^{(2)}, h_{GPS}^{(1)}, h_{GPS}^{(2)}, S_{GPS}, d_{GPS}\right) \leq VSWR_{GPS}^{\max}$$

$$(5)$$

where ($r_{GPS}^{(1)}$, $h_{GPS}^{(1)}$) and ($r_{GPS}^{(2)}, h_{GPS}^{(2)}$) denote the radius and the position of the lower [1] and of the upper [2] spiral turn of the helix, S_{GPS} is the distance between two adjacent turns of the spiral, and d_{GPS} its diameter.

Then, for each antenna subsystem the unknown physical parameter are obtained by maximizing a suitable cost function defined as follows:

$$\Omega_a\left(\underline{\gamma}_a\right) = \sum_{i=0}^{F-1}\sum_{v=0}^{V-1}\sum_{t=0}^{T-1}\left\{\max\left[0, \frac{\Phi_a\{t\Delta\theta, v\Delta\phi, i\Delta f\} - G_a^{\min}}{G_a^{\min}}\right]\right\} + \sum_{i=0}^{F-1}\left\{\max\left[0, \frac{VSWR_a^{\max} - \Psi_a\{i\Delta f\}}{VSWR_a^{\max}}\right]\right\}$$

$$(6)$$

where $\Delta\theta$, $\Delta\phi$, and Δf are sampling intervals, $\Phi_a\{t\Delta\theta, v\Delta\phi, i\Delta f\} = \Phi_a\left(\underline{\gamma}_a\right)$, $\Psi_a\{i\Delta f\} = \Psi_a\left(\underline{\gamma}_a\right)$, $\underline{\gamma}_a$ being the unknown array defining the physical characteristics of the a-th sub-system (i.e., $\underline{\gamma}_{SRS} = \{l_{SRS}, d_{SRS}\}$, $\underline{\gamma}_{GSM} = \{l_{GSM}^{(1)}, l_{GSM}^{(2)}, d_{GSM}, L, C\}$, and $\underline{\gamma}_{GPS} = \{r_{GPS}^{(1)}, r_{GPS}^{(2)}, h_{GPS}^{(1)}, h_{GPS}^{(2)}, S_{GPS}, d_{GPS}\}$).

Towards this end, a sequence of trial solutions is generated according to a stochastic multiple-agents strategy based on a particle swarm optimizer (PSO) [9]. The PSO is a robust stochastic search procedure inspired by the social behavior of insects swarms proposed by Kennedy and Eberhart in 1995 [10]. Thanks to its features in exploring complex search spaces, PSO has been employed with success in several problems in the

framework of applied and computational electromagnetics [11][9] as well as in the field of antenna synthesis [12][13][14].

Integrated-Antenna Optimization

Starting from the preliminary setup of each antenna sub-system defined upon the "*Single-Antenna Optimization*" phase, the last step deals with the integration in a single device. Once again the process is recast as an optimization problem and solved through the PSO-based approach. In this case, however, the overall system is considered as a single device, and the location of each antenna sub-system is added to the array of unknowns. Therefore, the arising cost function turns out to be:

$$\Omega(\underline{\gamma}) = \sum_{i=0}^{F-1}\sum_{v=0}^{V-1}\sum_{t=0}^{T-1}\left\{\max\left[0,\frac{\Phi\{t\Delta\theta,v\Delta\phi,i\Delta f\}-G^{\min}}{G^{\min}}\right]\right\} + \sum_{i=0}^{F-1}\left\{\max\left[0,\frac{VSWR^{\max}-\Psi\{i\Delta f\}}{VSWR^{\max}}\right]\right\}$$

(7)

where $G^{\min} = \bigcup_a G_a^{\min}$, $VSWR^{\max} = \bigcup_a VSWR_a^{\min}$, $\Phi\{t\Delta\theta,v\Delta\phi,i\Delta f\} = \Phi(\underline{\gamma})$, $\Psi\{i\Delta f\} = \Psi(\underline{\gamma})$, and $\underline{\gamma} = \left\{x_a^{(0)}, y_a^{(0)}, z_a^{(0)} = 0.0, \underline{\gamma}_a; \forall a\right\}$, $\left(x_a^{(0)}, y_a^{(0)}, z_a^{(0)} = 0.0\right)$ being the location of the *a*-th radiating element on the ground plane.

3.   EXPERIMENTAL VALIDATION

In this section, the results of the optimization procedure for designing a multifunction antenna operating in an automotive framework will be presented and assessed through an experimental as well as a numerical validation. The analyzed test case is characterized by the following constraints (defined according to the requirements resumed in Tab. I):

❑ $G_{SRS}^{\min}(\theta, f) = -3\,dBi$, $-85^o \leq \theta \leq -30^o$, $30^o \leq \theta \leq 85^o$, and $VSWR_{SRS}^{\max}(f) = 1.5$ in the frequency range from $f_{SRS}^{\min} = 406.015\,MHz$ up to $f_{SRS}^{\max} = 406.035\,MHz$;

❑ $G_{GSM}^{\min}(\theta, f)\big|_{\theta=\pm88.5^o} = -5\,dBi$ (with an average value of $-2\,dBi$ in the range $-90^o \leq \theta \leq -70^o$ and $70^o \leq \theta \leq 90^o$) and $VSWR_{GSM}^{\max}(f) = 1.5$ in the two

frequency bands between $f_{GSM}^{(1)\min} = 880\,MHz$ and $f_{GSM}^{(1)\max} = 960\,MHz$, and

between $f_{GSM}^{(2)\min} = 1.71\,GHz$ and $f_{GSM}^{(2)\max} = 1.99\,GHz$, respectively;

❑ $G_{GPS}^{\min}(\theta,f) = \begin{cases} -4\,dBi & \theta = \pm 70^o \\ 3\,dBi & \theta = 0^o \end{cases}$ and $VSWR_{GPS}^{\max}(f) = 2.0$ in the range

$f_{GPS}^{\min} = 1574.4\,MHz$ and $f_{SRS}^{\min} = 1576.4\,MHz$.

Moreover, the optimization has been performed under some hypotheses resumed in the following. Because of practical manufacturing constraints, the wire diameters has been fixed to 1 mm ($d_{SRS} = d_{GSM} = d_{GPS} = 1mm$) and the tuning device capacitor has been set to 1 pF. Furthermore, in order to comply with the project specifications, the following ranges of variations for the remaining geometrical parameters has been assumed:

❑ $\dfrac{1}{10} \le \dfrac{l_m}{\lambda_m} \le \dfrac{3}{8}$

where $m \in \{SRS, GSM/GPRS\,low\,band, GSM/GPRS\,upper\,band\}$, λ_m being the related free space wavelength;

❑ $10^{-12} \le L \le 10^{-6}\,[H]$;

❑ $0 \le r_{GPS}^{(1)} \le 50[mm]$, $\quad 0 \le r_{GPS}^{(2)} \le 5[mm]$, $\quad 0 \le h_{GPS}^{(1)} \le 3[mm]$, $\quad 0 \le h_{GPS}^{(2)} \le 8[mm]$,

$1 \le S_{GPS} \le 20[mm]$.

Figure 1 shows the geometry of the resulting multifunction antenna as obtained at the end of the optimization procedure. The lengths of the two monopole antennas are equal to $l_{SRS} = 175$ mm (SARSAT band) and to 53 mm (double-band GSM/GPRS subsystem). The tuning device necessary for the double-band operation of the GSM/GPRS monopole is located along the corresponding metallic wire at 39 [mm] from the reference ground plane. The conical spiral antenna has the following geometrical characteristics: $r_{GPS}^{(1)} = 46.1$ mm and $r_{GPS}^{(2)} = 0.1$ mm, $h_{GPS}^{(1)} = 35$ mm and $h_{GPS}^{(2)} = 65$ mm, and $S_{GPS} = 13.6$ mm.

As can be observed, the two monopole antennas are located in the middle of the conical Archimedean spiral according to the geometric constraints on the maximum volume of the integrated antenna and for reducing the mutual coupling phenomena in working frequency bands. More in detail, the locations of the SARSAT and GSM/GPRS monopoles obtained from optimization procedure are: ($x_{SRS} = -3.2\,cm$, $y_{SRS} = 1.85\,cm$)

and ($x_{GSM} = 2.43\,cm$, $y_{GSM} = -1.4\,cm$). As far as the GPS conical spiral antenna position is concerned, it has been fixed at ($x_{GPS} = 0$, $y_{GPS} = 0$) without loss of generality [Fig. 1(b)]. For completeness, the physical characteristics of the antenna sub-systems as well as of the whole multi-function antenna are summarized in Tab. II. The maximum vertical dimension is due to the SARSAT monopole ($l_{SRS} = 175\,mm$), a classical wire antenna perfectly compliant with an automotive application. The remaining part of the antenna belongs to a small sized conical volume characterized by a maximum height of about $65\,mm$.

In order to give an idea of the computational cost of the optimization procedure during the integration phase of the stand alone subsystems, Figure 2 shows a plot of the cost function (7). As can be noticed, the integration phase required approximately 230 iterations and each iteration took approximately 1 sec.

During the optimization processes (stand alone subsystems and integrated antenna), the antennas have been assumed on an infinite ground plane. In order to validate such an assumption, some preliminary verifications has been carried out with non optimized stand alone antennas. Simulated results obtained with an infinite ground plane and those obtained locating the antenna at the center of a ground plane with geometry similar to those of a car roof have been compared. The resulting differences have been considered acceptable in order to obtain the compliance of the final design with the project specifications. Moreover, as reported in literature [15], comparing the maximum wavelength (0.74 m) with the minimum dimensions of a roof of a generic car ($\cong 1.2 \times 2.0\ m^2$), the maximum expected difference for the gain values at horizon is approximately equal to 4 dB.

For an experimental validation, the performance of the multi-function antenna obtained from different numerical models of the structure and those measured from the prototype shown in Fig. 3 have been compared. Both gain and VSWR measurements have been acquired in an anechoic chamber where a calibrated log-periodic antenna for SARSAT and GSM/GPRS ($f_{GSM}^{(1)} = 930\,MHz$) bands and a calibrated double-ridged horn antenna for GSM/GPRS ($f_{GSM}^{(2)} = 1.85\,GHz$) band have been used. During the experimental tests,

the antenna prototype has been equipped with a 90×140 cm^2 ground plane. Moreover, in order to verify the circular polarization of the GPS sub-system, a second sample of the device has been built to measure right-hand-circular-polarization gain values. As far as the VSWR measurements are concerned, the standing wave ratio values have been acquired by means of a scalar network analyzer.

Far-field conditions in the whole frequency range have been considered, since the measurement distance was always greater than $50 D^2/\lambda$, D being the largest antenna dimension and λ the free-space wavelength at the working frequency.

Figure 4 shows the behavior of the gain function [Figs. 4(a)-4(b)] as well as of the VSWR [Figs. 4(c)-4(d)] for the COSPAS-SARSAT band. For comparison purposes, the values simulated with the MoM-based [16] and the FDTD-based [17] numerical simulators are reported, as well. Moreover, according to the multi-phase design procedure, the results of the stand alone antenna sub-system [Figs. 4(a)-4(c)] and of the integrated device Figs. [4(b)-4(d)] are analyzed. More in detail, Figs. 4(a)-4(b) show the gain along a vertical plane ($\phi = 0°$) in the angular range $\theta \in \left[-85^o, -30^o\right] \cup \left[30^o, 85^o\right]$.

The omni directional properties of the integrated antenna in this frequency band have been numerically verified. The measured values highlight a good behavior of the antenna in the COSPAS-SARSAT band as suggested by the numerical simulations, since the gain values are more than $3\,dB$ in the overall elevation range. A good agreement between measured and simulated data is shown in Figs. 4(c)–4(d), confirming the effectiveness of the design process in fitting the project specifications.

As for COSPAS/SARSAT, a similar analysis has been carried out for the GSM/GPRS bands. The results of such a study are reported in Fig. 5 for the $\phi = 162^o$ vertical-cut plane (around the central frequency of $f_{GSM}^{(1)} = 930\,MHz$) and in Fig. 6 for the ($\phi = 150^o$) vertical-cut plane (around the central frequency of $f_{GSM}^{(2)} = 1.85\,GHz$). From Figs. 5($a$)-5($b$), it turns out that the gain of the synthesized antenna is of about $4\,dB$ better than the specifications in the whole elevation range $\theta \in \left[-90^o, -70^o\right] \cup \left[70^o, 90^o\right]$.

Furthermore, it can be noticed [Fig. 5(b)] that, because of the mutual interferences among the antenna sub-systems, the gain function of the integrated antenna doesn't

present the null-point at $\theta = 0^o$, which appears when the stand alone optimized monopole is considered [Fig. 5(a)]. The project specifications are also satisfied in the upper frequency band as confirmed by Figs. 6(a) and 6(b). Only in a limited portion of the angular range (i.e., $\theta \cong \pm 90^o$), the measured values are slightly under the guidelines. Such an event is probably caused by the limited extent of the ground plane in the multifunction antenna prototype as confirmed from the numerical simulations where an infinite metallic surface has been considered. However, the gain performance has been considered compliant with the project specifications since the reference value (equal to $-2.0\,dBi$) has been assumed as a minimum linear average in overall elevation range, while $\left. G_{GSM}(\theta, f) \right|_{\theta = \pm 88.5^o} = -3\,dBi$ (being $\left. G_{GSM}^{\min}(\theta, f) \right|_{\theta = \pm 88.5^o} = -5\,dBi$). For completeness, the results concerned with the VSWR are displayed in Figs. 5(c)-5(d) and Figs. 6(c)-6(d).

Finally, the GPS band has been analyzed. Fig. 7 shows measured and simulated gain values along the vertical planes $\phi = 0^o$ and $\phi = 90^o$, respectively. In both the vertical planes [$\phi = 0^o$ - Figs. 7(a)-7(b); $\phi = 90^o$ - Figs. 7(c)-7(d)] and for both the antenna configurations [stand alone - Figs. 7(a)-7(c); integrated - Figs. 7(b)-7(d)], the measured values are compliant with the specifications at $\theta = 0^o$ [$G_{GPS}(\theta, f) - G_{GPS}^{\min}(\theta, f) \approx 1\,dB$].

On the contrary, the gain of the prototype presents a sharp slope in the lower part of the angular range (i.e., $\theta < -70^o$ and $\theta > 70^o$) and it does not satisfy the project requirements. In particular, at $\theta = \pm 70^o$ the gain value of the integrated antenna turns out to be of about $6\,dB$ under the specifications. However, such a result can be considered as acceptable since a pre-amplification of about $28\,dB$ is required because of the weak level of the GPS signals at the earth surface (approximately, $-130\,dBm$). As a matter of fact, the microwave circuit (shown in Fig. 8) composed by a GPS band pass filter and a low noise amplifier has been designed and integrated in the multi-function antenna. A balun with an impedance ratio equal to 1:4 has been placed between the balanced GPS port of the antenna and the input of the microwave circuit. The balun transformer is needed because of the input impedance of the conical spiral sub-system

(of about $200\,\Omega$). Moreover, a matching network has been inserted in the microwave circuit, but the compliance to requirements at the integrated antenna input port is guaranteed by the output impedance of the employed low noise preamplifier in the circuit ($VSWR_{GPS}^{\max} = 1.5$). Figs. 9(*a*)-9(*b*) show the achieved VSWR by assuming the presence of a 4:1 impedance transformer inserted at the input port of the GPS sub-system.

As far as the polarization state of the GPS antenna is concerned, the similar behavior of the gain function measured at $\phi = 0^o$ and at $\phi = 90^o$ can be considered an experimental indication of the circular polarization. For completeness, another validation test has been performed by repeating the measurements of the multifunction antenna prototype with a double ridged horn antenna, which operates in the GPS band and characterized by a linear polarization. As can be observed in Fig. 10, the values measured in the two orthogonal planes are equivalent in large part of the angular range. Furthermore, as expected, there is a difference of about $3\,dB$ between the values measured with two circular polarized antennas and those collected with a linearly-polarized antenna in the measurement set-up.

From the experimental analysis of the gain functions, the following considerations can be inferred. Because of the integrated antenna is not symmetric about the *z*-axis, even though an infinite ground plane has been considered, the gain function of the overall system presents some variations in the *xy*-plane. Except for the SARSAT band, for which omni directional properties have been numerically as well as experimentally verified, the maximum gain variations concerned with the GSM/GPRS bands have been numerically found to be $+5.68$ dB for the GSM upper band at $\theta = 90^o$ (with respect to the value in the "worst" vertical-cut plane $\phi = 150°$ shown in Fig. 6) and $+4.17$ dB for the GSM lower band at $\theta = 70^o$ (with respect to the value in the "worst" vertical-cut plane $\phi = 162°$ shown in Fig. 5). As far as GPS band is concerned, even though only two orthogonal vertical-cut planes have been presented ($\phi = 0^o$, $\phi = 90^o$), an almost omni-directional behavior with negligible variations in the gain function along the *xy*-plane has been numerically verified.

Finally, in addition to the experimental validation in a semi-anechoic chamber, some functional tests have been carried out. To further assess the GPS functionalities, the multifunction antenna has been connected to a GPS receiver and its behavior has been compared with that of an analogous receiver equipped with a patch antenna. When placed in the same area, the receiver equipped with the multi-function antenna prototype received one or two satellite signals more than the receiver equipped with a patch antenna.

4.   CONCLUSIONS

In this paper the design of an integrated multi-function antenna for an automotive rescue management system has been described. Due to several electrical and geometrical constraints fixed by the project specifications, the design has been faced by means of a multi-phase optimization procedure. The design process as well as the resulting multi-function antenna prototype has been validated through experimental and numerical tests. The comparison of numerical and experimental results in terms of gain and VSWR as well as the verification of the compliance with the project constraints, have confirmed the effectiveness of the proposed design procedure.

Future activities will be aimed at applying the proposed approach to the integration of different kind of antennas for various wireless services.

REFERENCES

[1]   N. Padros, J. I. Ortigosa, J. Baker, M. F. Iskander, "Comparative study of high-performance GPS receiving antenna designs," *IEEE Trans. Antennas Propagat.*, vol. 45, pp. 698-706, Apr. 1997.

[2]   J. D. Kraus, *Antennas*. New York: McGraw-Hill, 1988

[3]   C. A. Balanis, *Antenna Theory: Analysis and Design*. New York: Wiley, 1996.

[4]   D. M. Sazonov, *Microwave circuits and antennas*. Moscow: Mir Publisher: Moscow, 1998.

[5]   W. L. Curtis, "Spiral antennas," *IRE Trans. Antennas Propagat*., vol. 8, pp. 298-306, May 1960.

[6]   J. A. Kaiser, "The archimedean two-wire spiral antennas," *IRE Trans. Antennas Propagat*., vol. 8, pp. 312-323, May 1960.

[7]   E. Gschwendtner and W. Wiesbeck, "Low-cost spiral antenna with dual-mode radiation pattern for integrated radio services," *Proc. Millenium Conf. Antennas Propagat. (AP2000)*, Davos, Switzerland, April, 9-14, 2000.

[8]   Y. Zhang and H. T. Hui, "A printed hemispherical helical antenna for GPS receiver," *IEEE Microwave Wireless Components Lett.*, vol. 15, pp. 10-12, Jan. 2005.

[9]   A. Massa and M. Donelli, "A computational approach based on a particle swarm optimizer for microwave imaging of two-dimensional dielectric scatterers," *IEEE Trans. Microwave Theory Tech.*, in press.

[10]   J. Kennedy, R. C. Eberhart, and Y. Shi, *Swarm Intelligence*. San Francisco: Morgan Kaufmann Publishiers, 2001.

[11]   J. R. Robinson and Y. Rahmat-Samii, "Particle swarm optimization in electromagnetics," *IEEE Trans. Antennas Propagat.*, vol. 52, pp. 771-778, Mar. 2004.

[12] Y. Rahmat-Samii, "Frontiers in evolutionary optimization techniques applied to antenna designs: genetic algorithms and particle swarm optimization," in *Proc. 13th Int. Symp. Antennas* (*JINA 2004*), Nice, France, 8-10 Nov. 2004.

[13] D. W. Boringer and Douglas H. Werner, "Particle swarm optimization versus genetic algorithms for phased array synthesis," *IEEE Trans. Antennas Propagat.*, vol. 52, pp. 771-779, Mar. 2004.

[14] M. Donelli et *al.*, "An innovative computational approach based on a particle swarm strategy for adaptive pahsed-arrays control," submitted to *IEEE Trans. Antennas Propagat.*

[15] M.M. Weiner, S. P. Cruze, C. Li and W. J. Wilson, *Monopole elements on circular ground planes*, Artech House, 1987.

[16] G. J. Burke and A. J. Poggio, *Numerical Electromagnetics Code (NEC) - Method of Moments*. Lawrence Livermore Nat. Lab., Livermore, CA, Tech. Rep. UCID-18834, 1981.

[17] D. M. Sullivan, *Electromagnetic Simulation using the FDTD Method*. IEEE Press Series on RF and Microwave Technology, New York, 2000.

FIGURE CAPTIONS

Figure 1. Geometry of the multi-function antenna: (*a*) side view and (*b*) top view.

Figure 2. Behavior of the cost function (7) versus the iteration number.

Figure 3. Photograph of the prototype of the multi-function antenna.

Figure 4. Multi-function antenna results for COSPAS-SARSAT band: (*a*) measured and simulated gain of the stand alone monopole along a vertical plane, (*b*) measured and simulated gain of the integrated multifunction antenna along a vertical plane, (*c*) measured and simulated VSWR of the stand alone optimized monopole, (*d*) measured and simulated VSWR of the optimized integrated multifunction antenna.

Figure 5. Multi-function antenna results for GSM/GPRS lower band: (*a*) measured and simulated gain of the stand alone double-band monopole along a vertical plane, (*b*) measured and simulated gain of the integrated multifunction antenna along the "worst" vertical plane $(\phi = 162^{o})$, (*c*) measured and simulated VSWR of the stand alone double-band monopole, (*d*) measured and simulated VSWR of the integrated multifunction antenna.

Figure 6. Multi-function antenna results for GSM/GPRS upper band: (*a*) measured and simulated gain of the stand alone double-band monopole along a vertical plane, (*b*) measured and simulated gain of the integrated multifunction antenna along the "worst" vertical plane $(\phi = 150^{o})$, (*c*) measured and simulated VSWR for the stand alone double-band monopole, (*d*) measured and simulated VSWR of the optimized integrated multifunction antenna.

Figure 7. Multi-function antenna results for GPS: (*a*) measured and simulated gain of the stand alone conical spiral antenna at $\phi = 0^{o}$, (*b*) measured and simulated gain of the integrated multifunction antenna at $\phi = 0^{o}$, (*c*) measured and simulated gain of the stand alone conical spiral antenna at $\phi = 90^{o}$, (*d*) measured and simulated gain of the integrated multifunction antenna at $\phi = 90^{o}$.

Figure 8. Details of the multi-function antenna prototype.

Figure 9. Multi-function antenna results for GPS: (*a*) measured and simulated VSWR of the stand-alone conical spiral antenna, (*b*) measured and simulated VSWR of the integrated multifunction antenna.

Figure 10. Multi-function antenna: measured gain in two orthogonal vertical planes ($\phi = 0^o$, $\phi = 90^o$) for the GPS band with a linear polarized antenna.

TABLE CAPTIONS

Table I.   Multi-function antenna project specifications.

Table II.   Geometric characteristics of the multi-function antenna prototype.

| MULTI-FUNCTION ANTENNA SPECIFICATIONS				
WIRELESS LINK	**FREQ. [MHz]**	**POLARIZATION**	**GAIN**	**VSWR (related to 50 Ω)**
COSPAS - SARSAT	406.015 – 406.035	Linear (vertical)	$-3.0\,dBi$ min ($-85° \leq \theta \leq -30°$, $30° \leq \theta \leq 85°$)	1.5 max
GSM/GPRS	880 – 960	Linear (vertical)	$-5.0\,dBi$ min at $\theta = \pm88.5°$ $-2.0\,dBi$ min on average ($-90° \leq \theta \leq -70°$, $70° \leq \theta \leq 90°$)	1.5 max at $\dfrac{\left\| f_{GSM}^{(1)\min} - f_{GSM}^{(1)\max} \right\|}{2}$ 1.5 max in the 30% of the frequency band
	1710 - 1990	Linear (vertical)	$-5.0\,dBi$ min at $\theta = \pm88.5°$ $-2.0\,dBi$ min on average ($-90° \leq \theta \leq -70°$, $70° \leq \theta \leq 90°$)	1.5 max at $\dfrac{\left\| f_{GSM}^{(2)\min} - f_{GSM}^{(2)\max} \right\|}{2}$ 1.5 max in the 30% of the frequency band
GPS	1574.4 – 1576.4	RHCP	$3.0\,dBi$ min at $\theta = 0°$ $-4.0\,dBi$ min at $\theta = \pm70°$ (with a preamplification of $28\,dB$)	2.0 max

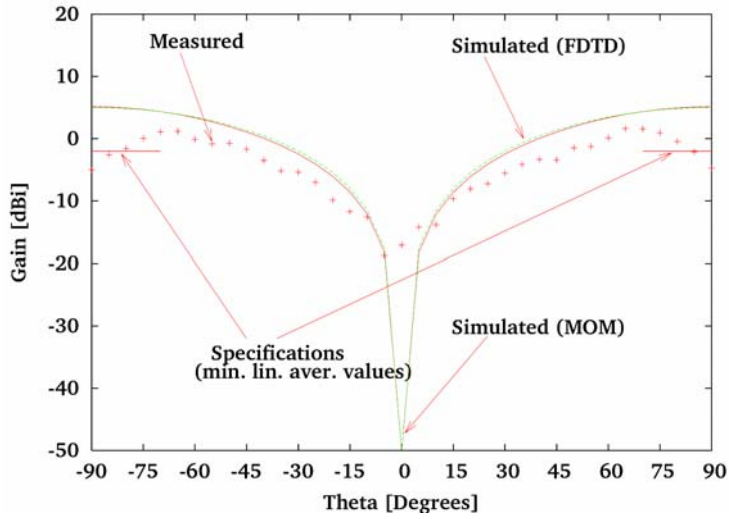**Table 1 – R.Azaro et *al.*,** "Optimized Design of a multi-function/multi-band antenna ..."

MULTI-FUNCTION ANTENNA GEOMETRICAL DIMENSIONS			
	Max X [mm]	**Max Y [mm]**	**Max Z [mm]**
COSPAS – SARSAT subsystem	0.5 (wire radius)	0.5 (wire radius)	175 (monopole length)
GSM/GPRS subsystem	0.5 (wire radius)	0.5 (wire radius)	53 (monopole length)
GPS subsystem	46 (max x of the lower spiral turn)	40 (max y of the lower spiral turn)	65 (height of the top of the spiral)
MULTI-FUNCTION ANTENNA	46 (X of GPS subsyst.)	40 (Y of GPS subsyst.)	175 (Z of SARSAT monopole)

Table 2 – R.Azaro et *al.*, "Optimized Design of a multi-function/multi-band antenna ..."
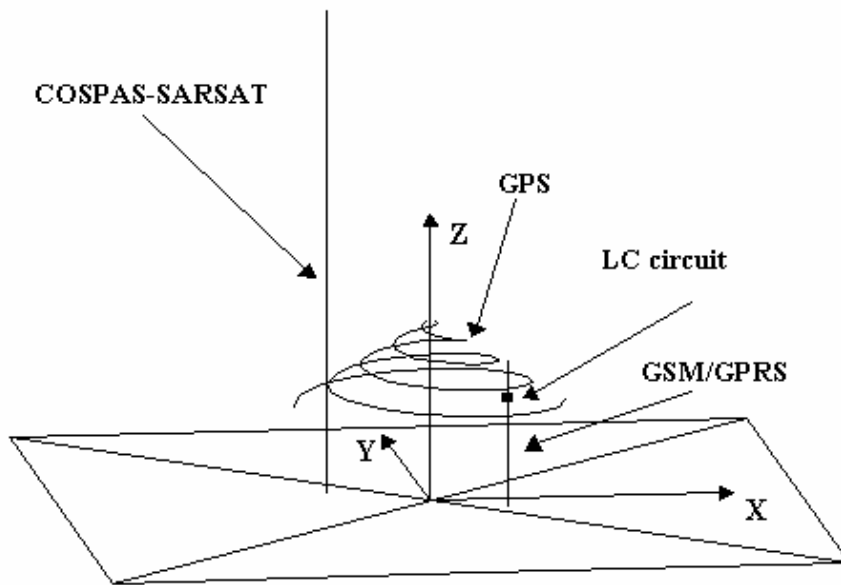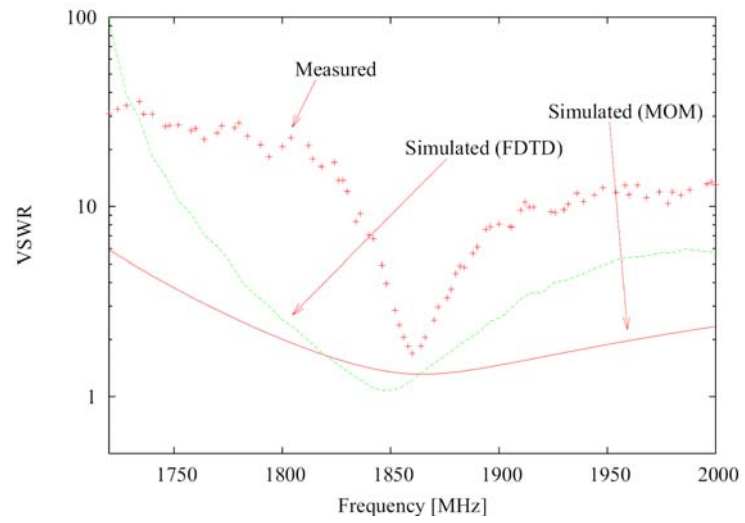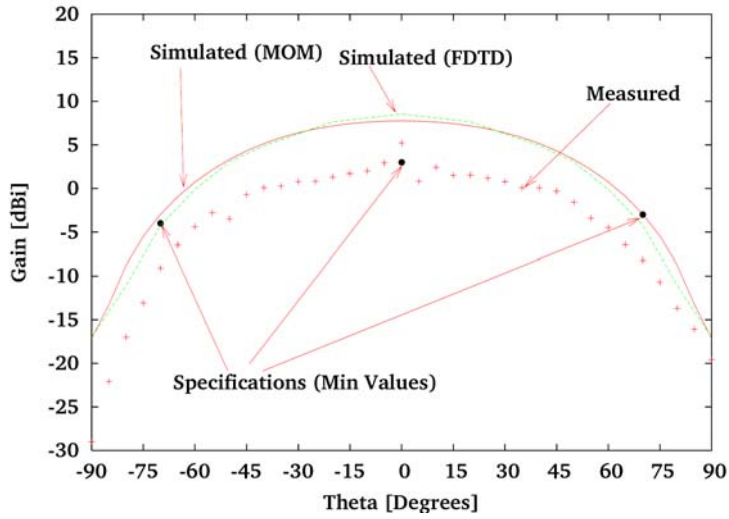
(*a*)
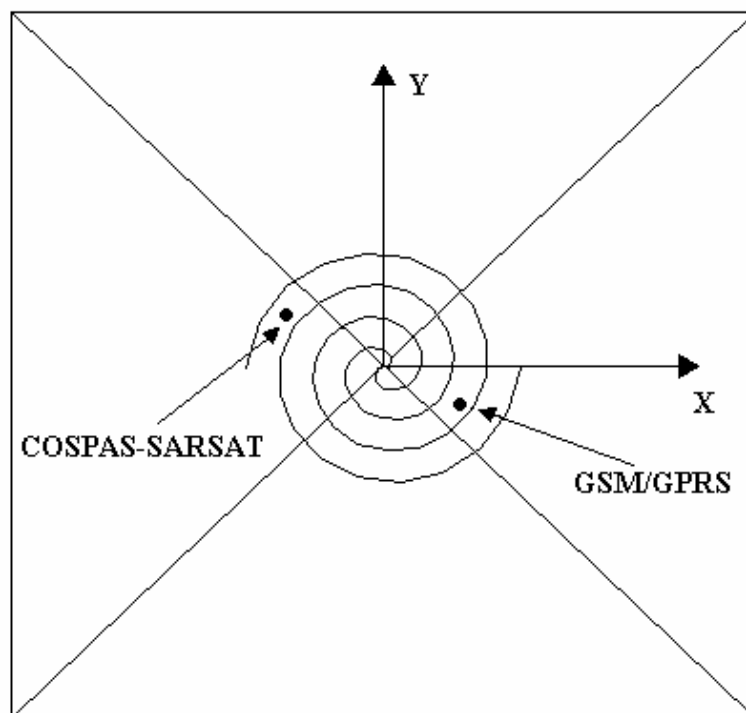
(*b*)

Fig. 1 – R.Azaro et *al.*, "Optimized Design of a multi-function/multi-band antenna ..."
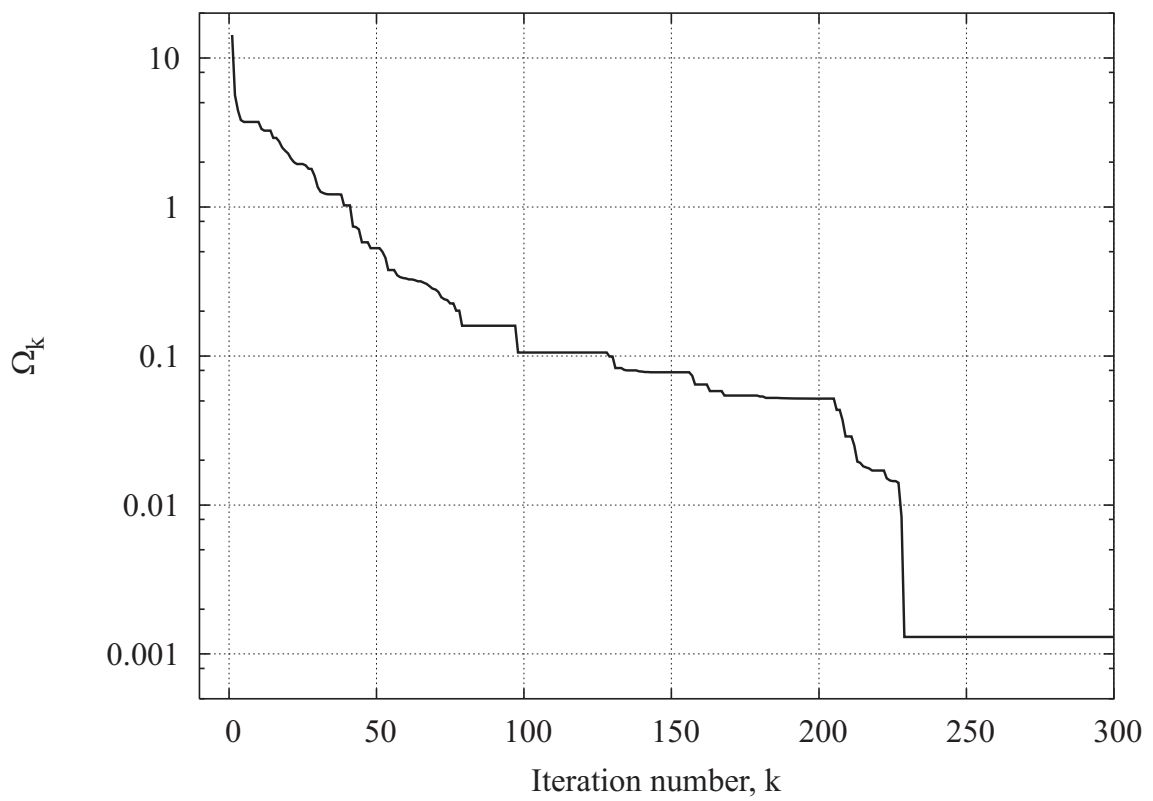
Fig. 2 – R.Azaro et *al.*, "Optimized Design of a multi-function/multi-band antenna ..."
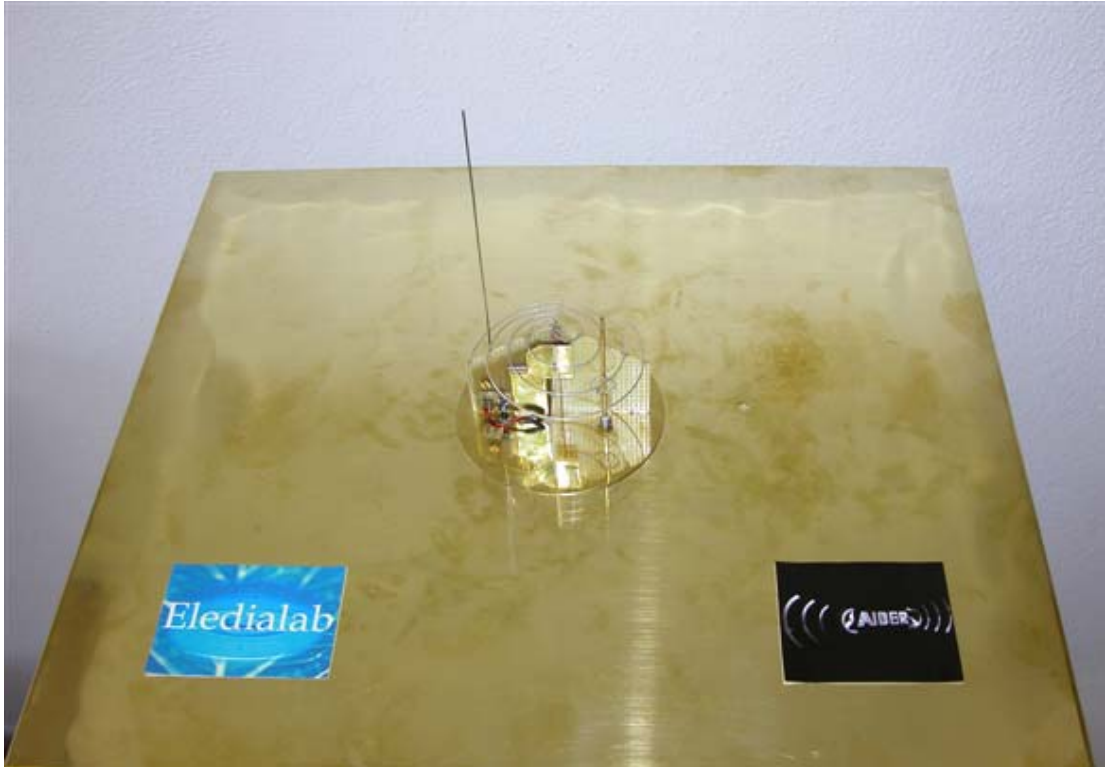
Fig. 3 – R.Azaro et *al.*, "Optimized Design of a multi-function/multi-band antenna ..."
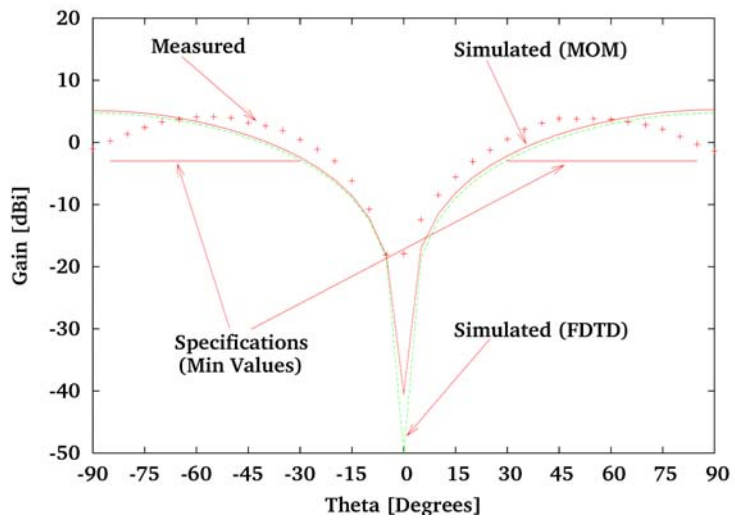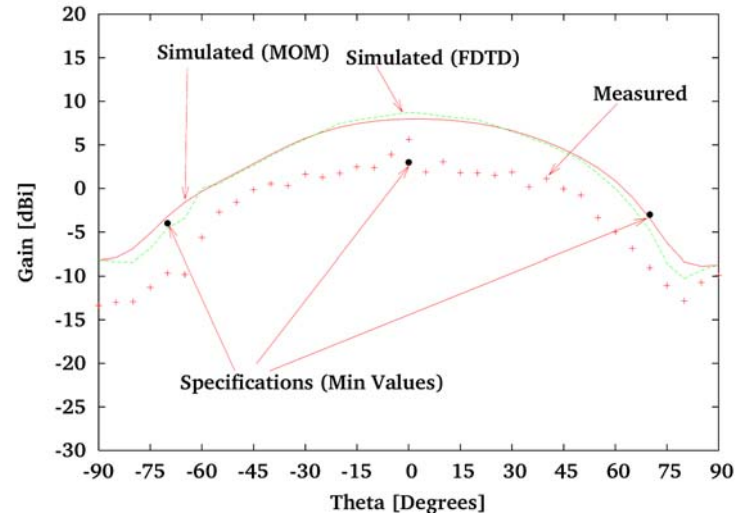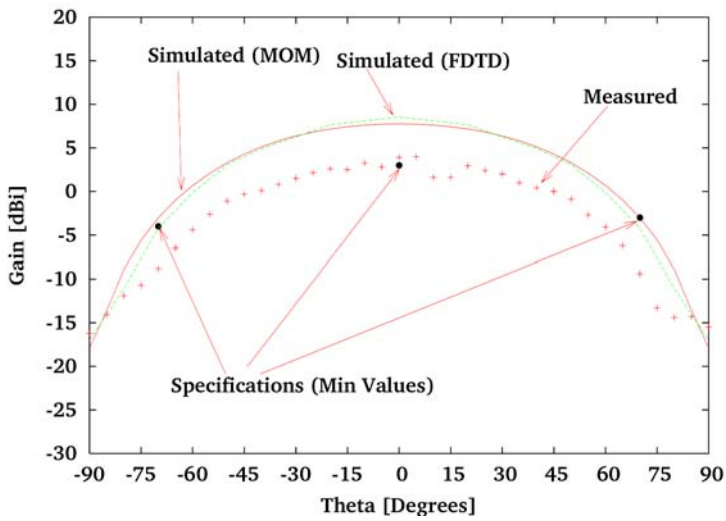
(*a*)
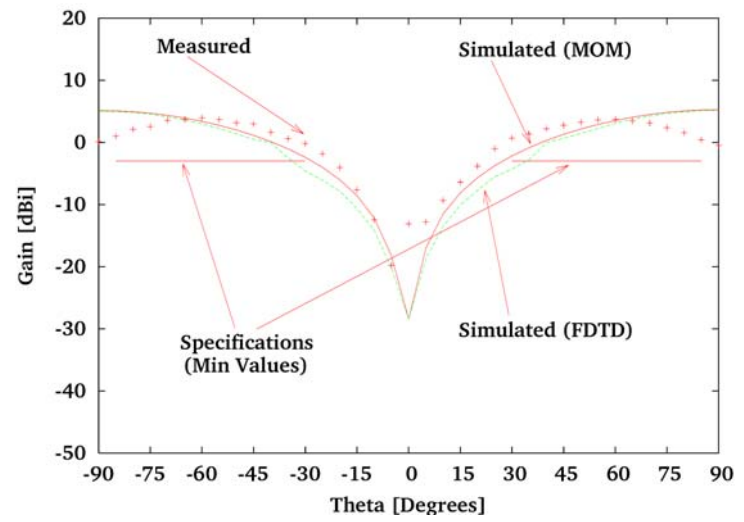
(*b*)
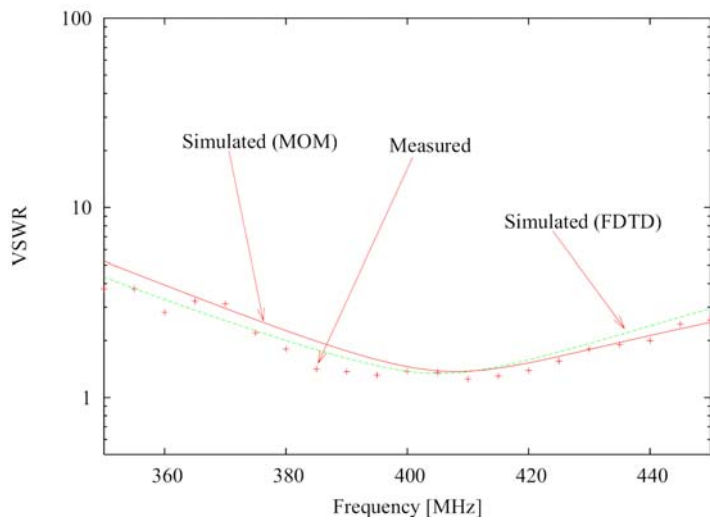
(*c*)
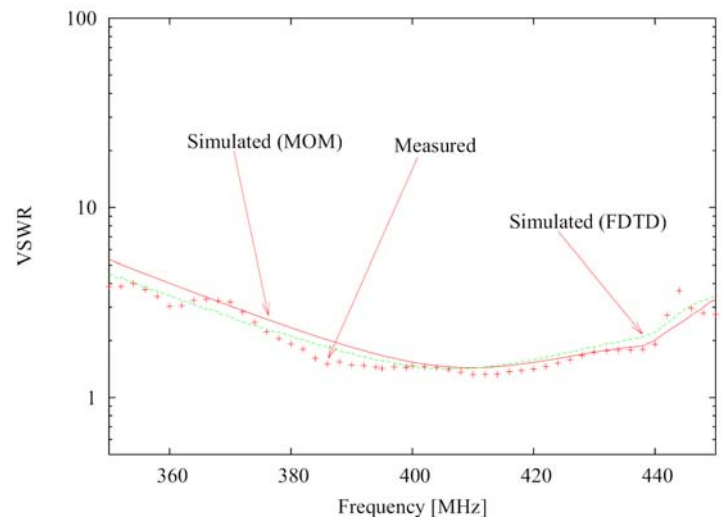
(*d*)

Fig. 4 – R.Azaro et *al.*, "Optimized Design of a multi-function/multi-band antenna ..."
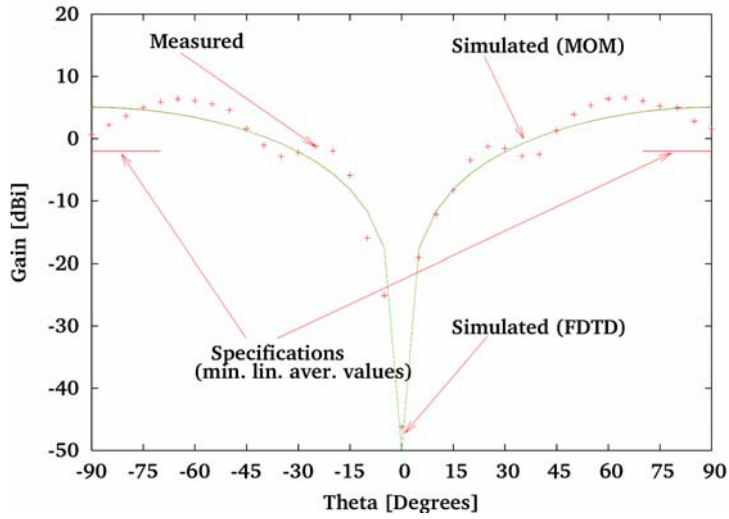
(*a*)
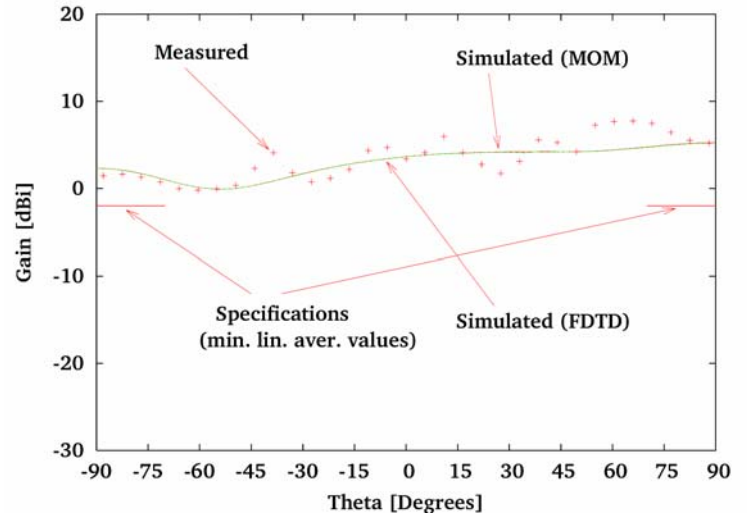
(*b*)
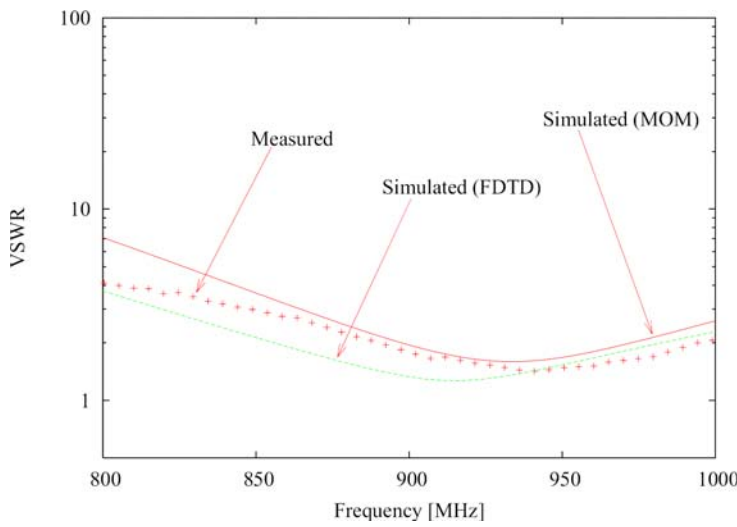
(*c*)
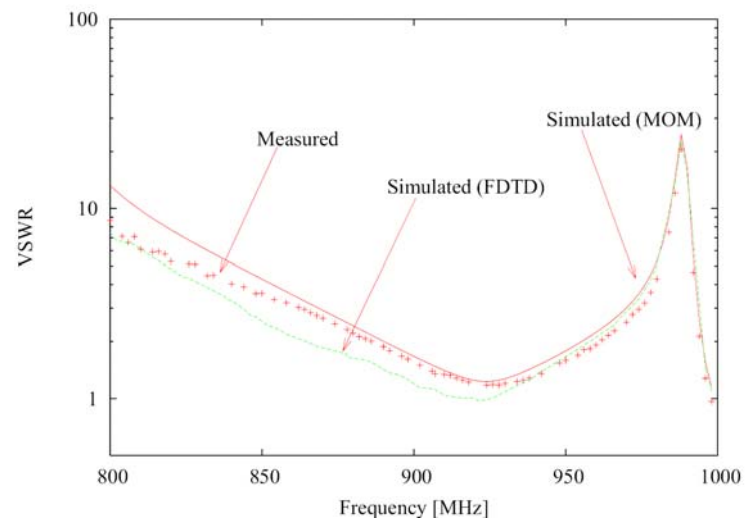
(*d*)

Fig. 5 – R.Azaro et *al.*, "Optimized Design of a multi-function/multi-band antenna ..."
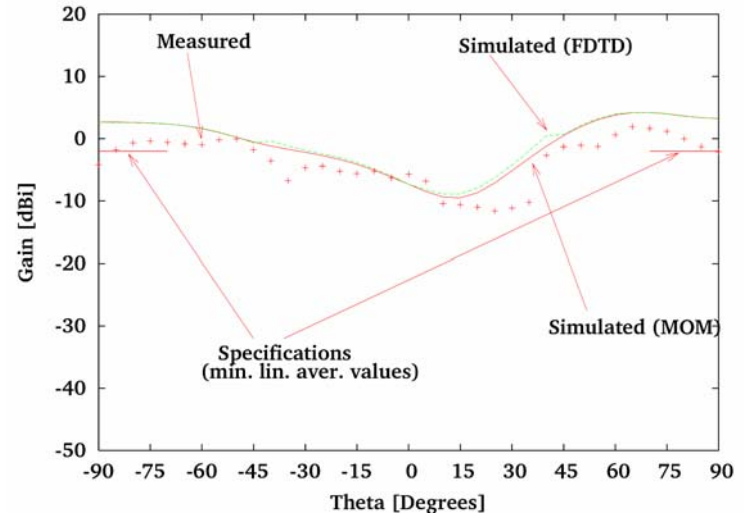
(*a*)   (*b*)
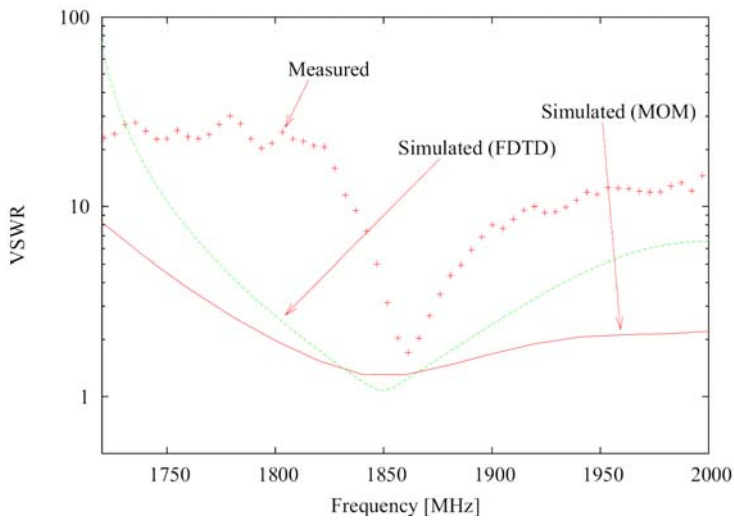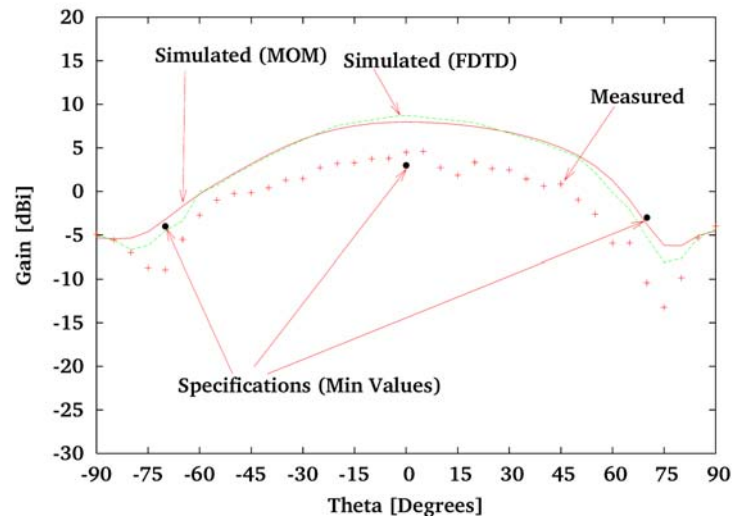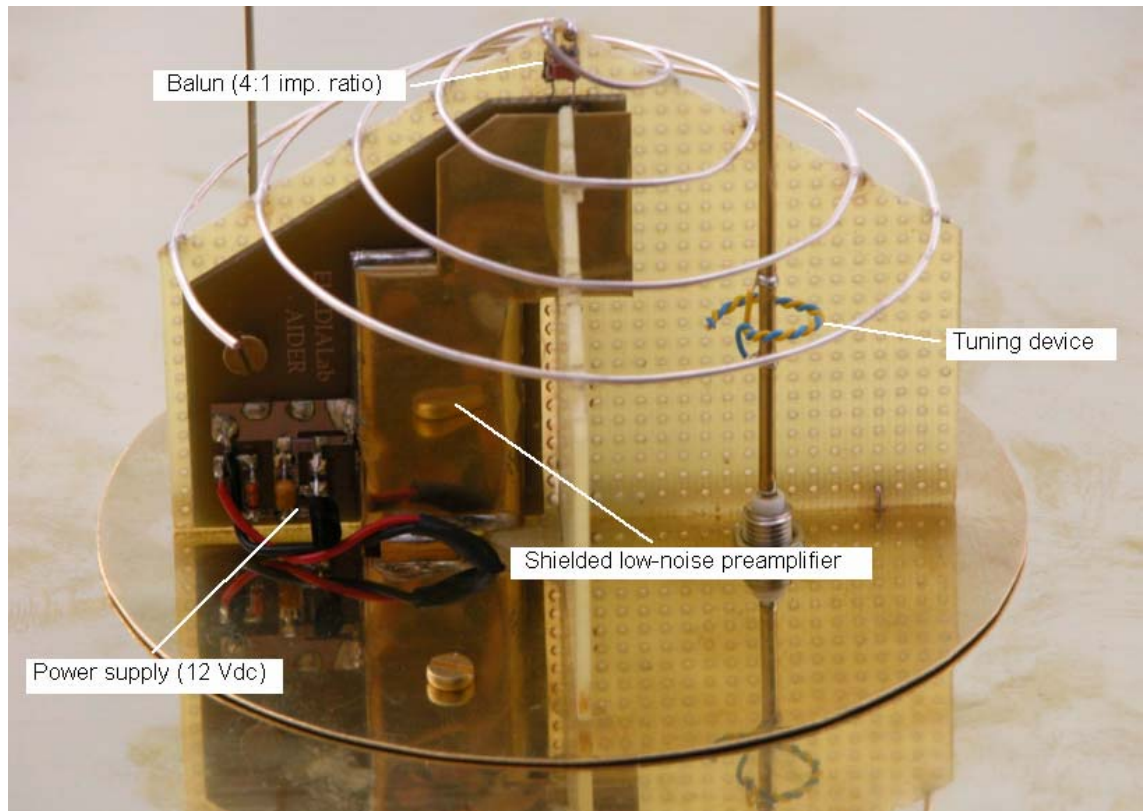

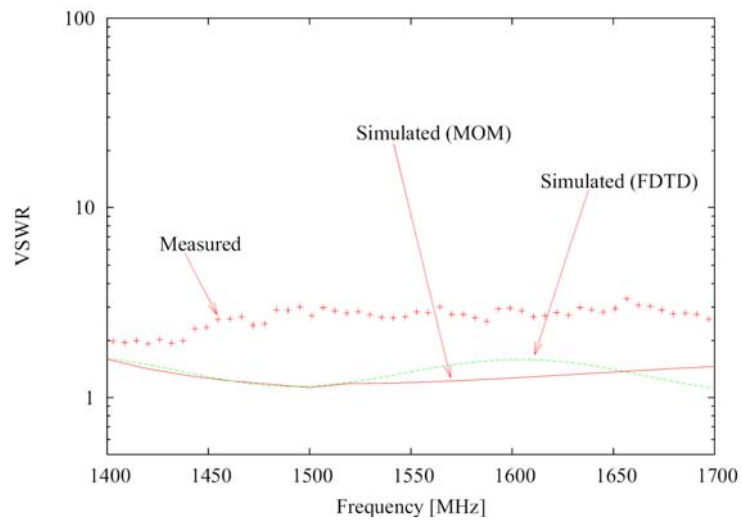(*c*)   (*d*)

Fig. 6 – R.Azaro et *al.*, "Optimized Design of a multi-function/multi-band antenna ..."

(*a*)
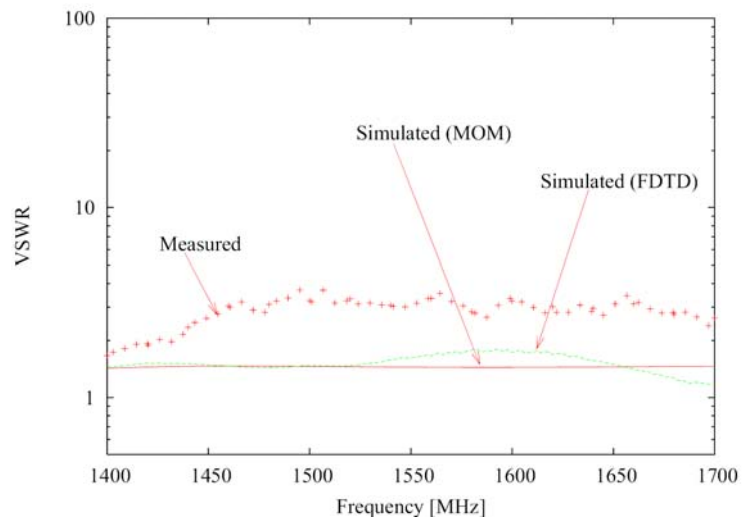

(*b*)

(*c*)

(*d*)

Fig. 7 – R.Azaro et *al.***,** "Optimized Design of a multi-function/multi-band antenna ..."

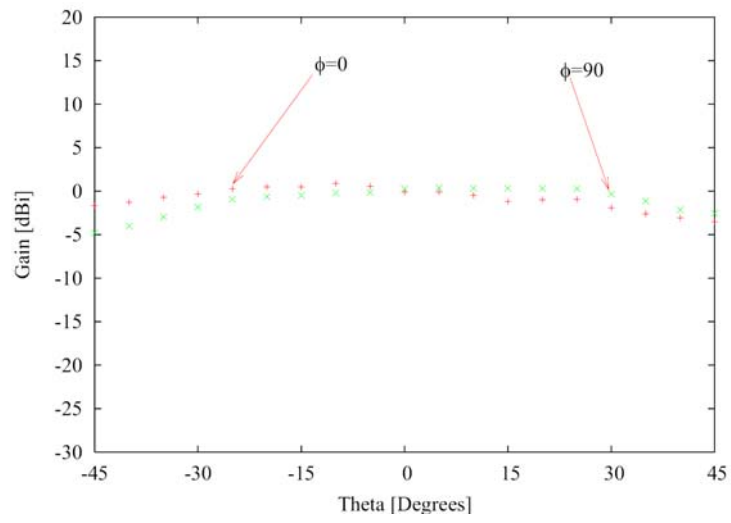**Fig. 8 – R.Azaro et *al.*,** "Optimized Design of a multi-function/multi-band antenna ..."

(*a*)

(b)

Fig. 9 – R.Azaro et *al.*, "Optimized Design of a multi-function/multi-band antenna ..."

Fig. 10 – R.Azaro et *al.***,** "Optimized Design of a multi-function/multi-band antenna ..."